ADVANCED ENERGY MATERIALS
www.advenergymat.de

Materials Views
www.MaterialsViews.com

Increase in the Figure of Merit by Cd-Substitution in $Sn_{1-x}Pb_xTe$ and Effect of Pb/Sn Ratio on Thermoelectric Properties

*Mi-Kyung Han, Xiaoyuen Zhou, Ctirad Uher, Sung-Jin Kim, and Mercouri G. Kanatzidis**

The effects of Cd-doping on the thermoelectric properties of $Sn_{1-x}Pb_xTe$ are investigated and compared to the properties of the corresponding $Sn_{1-x}Pb_xTe$ solid solutions. The addition of Cd results in a reduction in the carrier concentration and changes in the physical properties, as well as in the conduction type of $Sn_{1-x}Pb_xTe$. A significant increase in the power factor accompanied by a reduction in the thermal conductivity result in a higher figure of merit (ZT) for $(Sn_{1-x}Pb_x)_{0.97}Cd_{0.03}Te$ than that of undoped $Sn_{1-x}Pb_xTe$. The maximum ZT (~0.7) values are observed for p-type material with x = 0.36 at 560 K. Much higher values (ZT ~ 1.2 at 560 K for x = 0.73) are obtained on n-type samples.

1. Introduction

Thermoelectric materials can convert waste heat directly into electrical energy, and have the potential to play an important role in energy conservation and generation.[1,2] The performance of a thermoelectric material is defined by the figure of merit $ZT = (S^2\sigma\ \kappa^{-1})T$; where S is the Seebeck coefficient (or thermopower), σ electrical conductivity, κ thermal conductivity, and T is the temperature. The product ($S^2\sigma$) is called the power factor. All parameters (S, σ, and κ) in ZT vary with carrier concentration. Therefore, controlling carrier concentration is an essential first step for optimizing the ZT values.

Among numerous materials, lead telluride (PbTe)-based alloys have attracted considerable attention because of their high melting point, good chemical stability, and low vapor pressure, in addition to a high figure of merit.[3–9] The PbTe–SnTe system forms a complete solid solution of $Sn_{1-x}Pb_xTe$ throughout the range $0 \le x \le 1$, and the synthesis and characteristic of this pseudo-binary system have been studied.[7–9] It has been shown that these solids are p-type semiconductors, and the physical properties, such as carrier concentration and energy gap can be tuned by changing the Sn/Pb ratio or by adding suitable dopants.[10,11]

In this paper we explored the introduction of small amounts of Cd in the $Sn_{1-x}Pb_xTe$ system. This was done substitutionally where the Cd atoms replaced a fixed number of Sn/Pb atoms in the structure. Our investigation of the thermoelectric properties of the $(Sn_{1-x}Pb_x)_{0.97}Cd_{0.03}Te$ system was motivated by a recent theoretical study suggesting a significant enhancement in the electronic density of states (DOS) near the band gap in PbTe or SnTe, when divalent atoms, such as Zn, Cd, Hg, Sn, and Ge are introduced on the metal sites of the rock salt structure.[12] This implies a possible enhancement of the power factor by forming resonant states close to the bottom of the conduction band and then populating these states with carriers using donor dopants.[12] Our efforts focused on preparing Cd containing $Sn_{1-x}Pb_xTe$ solid solutions and tuning their properties by changing the Pb/Sn ratio and the carrier concentration using PbI_2 as a donor dopant.

We investigated several $(Sn_{1-x}Pb_x)_{0.97}Cd_{0.03}Te$ ($0.10 \le x \le 0.87$) compositions. When x = 0.1–0.3, the $(Sn_{1-x}Pb_x)_{0.97}Cd_{0.03}Te$ system can be doped p-type semiconductors, and when x = 0.6–0.87, it can be doped n-type. Thermoelectric properties of x = 1 are reported separately.[13] Results of the synthesis, the characterization and thermoelectric properties of materials are presented. We show for the first time that introducing Cd in the structure of $Sn_{1-x}Pb_xTe$ solid solutions leads to an enhanced thermoelectric figure of merit.

2. Results and Discussion

X-ray diffraction patterns of $(Sn_{1-x}Pb_x)_{0.97}Cd_{0.03}Te$ ($0.10 \le x \le 0.87$) samples are shown in **Figure 1**(a). The patterns depict a single phase material crystallizing in a cubic NaCl-type structure. The lattice parameter as a function of Pb fraction is displayed in Figure 1(b). As shown in Figure 1(b), the lattice parameter increases with increasing x value, as expected based on the difference between the metallic radii of Pb (~147 pm) and Sn (~141 pm).[14] The linear dependence of the lattice parameter on the concentration x is consistent with Vegard's

Prof. M. G. Kanatzidis
Department of Chemistry
Northwestern University
Evanston, IL 60208, USA
E-mail: m-kanatzidis@northwestern.edu
Dr. M.–K. Han, Prof. S.–J. Kim
Department of Chemistry and Nano Science
Ewha Womans University
Seoul 120-750, Korea
X. Zhou, Prof. C. Uher
Department of Physics
University of Michigan
Ann Arbor, MI 48109, USA

DOI: 10.1002/aenm.201200083

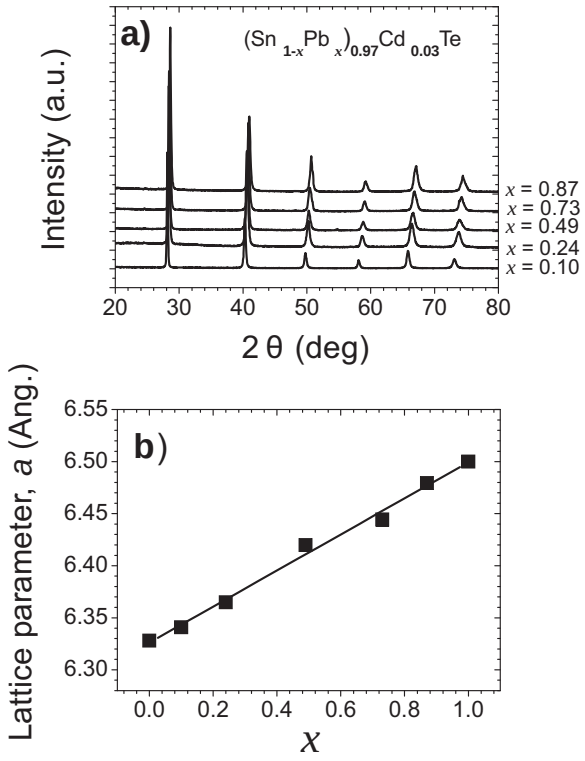

Figure 1. a) Power X-ray diffraction patterns of $(Sn_{1-x}Pb_x)_{0.97}Cd_{0.03}Te$ ($0.10 \le x \le 0.87$); b) Variation of the unit cell parameter as a function of x for the $(Sn_{1-x}Pb_x)_{0.97}Cd_{0.03}Te$ ($0 \le \times \le 1$).

law[15,16] and suggests the samples behave as typical solid solutions between SnTe and PbTe.[9] It has been known that the lattice parameter shows linear variation with carrier concentration in the binary $Sn_{1-x}Pb_xTe$ system,[17,18] whereas in Cd containing $Sn_{1-x}Pb_xTe$ system, no dependence of the lattice parameter upon carrier concentration was observed. The Cd atoms are believed to occupy Sn/Pb sites in the $(Sn_{1-x}Pb_x)_{0.97}Cd_{0.03}Te$ structure. The divalent nature of Cd implies that it is neither a donor nor an acceptor impurity. Therefore, the electron doping in the samples studied here comes from the n-type PbI_2 dopant. It is not clear at this stage how the small fraction of CdTe is accommodated in the $(Sn_{1-x}Pb_x)_{0.97}Cd_{0.03}Te$ structure. Recently, the effect of Cd substitution on the thermoelectric properties of PbTe in bulk $(PbTe)_{1-x}(CdTe)_x$ solid solution was explored.[13] The attempt to create Cd resonance levels in PbTe was unsuccessful, however, nanostructuring resulting from the low solubility of Cd in PbTe decreases the thermal conductivity values $\kappa \sim 1$ W m^{-1} K^{-1}, thus giving ZT of 1.2 at 720 K.

Figure 2 shows the composition dependence of the band gap. With increasing Pb concentration the energy gap initially decreases, goes through a minimum at around x = 0.61, and then increases with increasing Pb concentration. Similar observations were reported for the $Sn_{1-x}Pb_xTe$ system and the anomalous trend is understood in terms of the energy-band crossover.[16] A zero band gap in the $Sn_{1-x}Pb_xTe$ system was observed at the Sn-rich side of Pb0.4Sn0.6Te, whereas, for the Cd containing $Sn_{1-x}Pb_xTe$ system reported here, the band gap minimum was observed at the Pb-rich side of Pb0.61Sn0.36Cd0.03Te. This

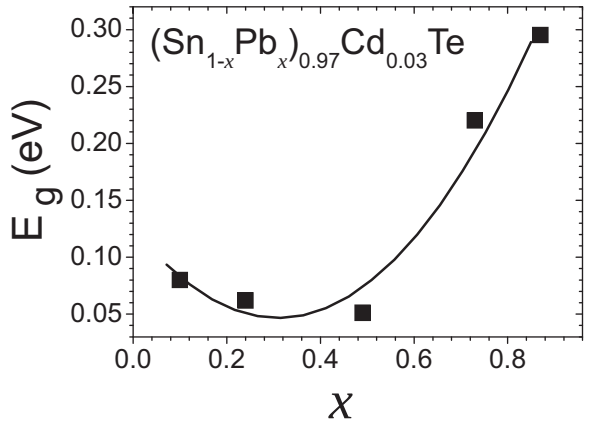

Figure 2. Composition dependence of the energy gap of $(Sn_{1-x}Pb_x)_{0.97}Cd_{0.03}Te$ ($0.10 \le x \le 0.97$).

may be attributed to perturbations in the band structure upon addition of Cd to the system. More detailed investigations of the electronic structure would be useful to clarify this point.

2.1. Charge Transport Properties

The electronic transport properties of the $(Sn_{1-x}Pb_x)_{0.97}Cd_{0.03}Te$ system can be tuned primarily through careful control of the Pb/Sn ratio. **Figure 3** illustrates the dependence of the electrical conductivity (σ) and Seebeck coefficient (S) at room temperature on x in the $(Sn_{1-x}Pb_x)_{0.97}Cd_{0.03}Te$ ($0.10 \le x \le 0.87$) system. On the Sn-rich side of the composition, a monotonic decrease in electrical conductivity was observed upon rising Pb concentration up to x = 0.61. It is well known that Sn-rich side of the $Sn_{1-x}Pb_xTe$ series is heavily doped with holes and this derives from the natural occurring Sn vacancies in the lattice. The trend in Figure 3 reflects the reduction of the hole carrier conduction as the number of Sn vacancies decreases with increasing Pb concentration. A further increase in the concentration of Pb above x > 0.6 led to an increase in the electrical conductivity and the appearance of a discontinuity in the trend.

The room temperature Seebeck coefficient behaves correspondingly. The Sn-rich solutions ($0.10 \le x \le 0.61$) show positive Seebeck coefficient which indicates that the majority of charge carriers are holes and it increases with x. In the Pb rich samples ($0.73 \le x \le 0.87$), the room temperature Seebeck coefficient is negative, indicating the majority of charge carriers are now electrons. The data are consistent with the Hall coefficient measurements where samples with a lower density of holes are likely to have higher Seebeck coefficients (see below). This implies that the change in behavior at x ~ 0.6 is coupled to the band crossover effect.[16] The discontinuities observed in the electrical conductivity and Seebeck coefficient data around x = 0.6 ~ 0.7 are commensurate with the trend reversal observed in the band gap of these material around the same x value (See Figure 2).

The temperature dependence of electrical conductivity (σ) and Seebeck coefficient data for $(Sn_{1-x}Pb_x)_{0.97}Cd_{0.03}Te$ ($0.10 \le x \le 0.87$) are shown in **Figure 4** and **Figure 5**, respectively.

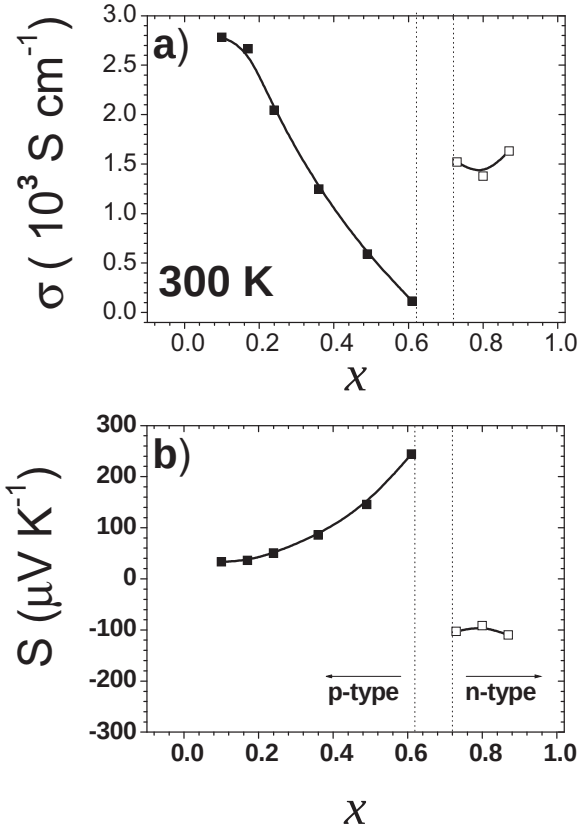

Figure 3. Composition dependence of (a) the room temperature electrical conductivity (σ); b) Seebeck coefficient (S) of $(Sn_{1-x}Pb_x)_{0.97}Cd_{0.03}Te$ ($0.10 \le x \le 0.97$) with 0.055 mol% PbI_2 as dopant.

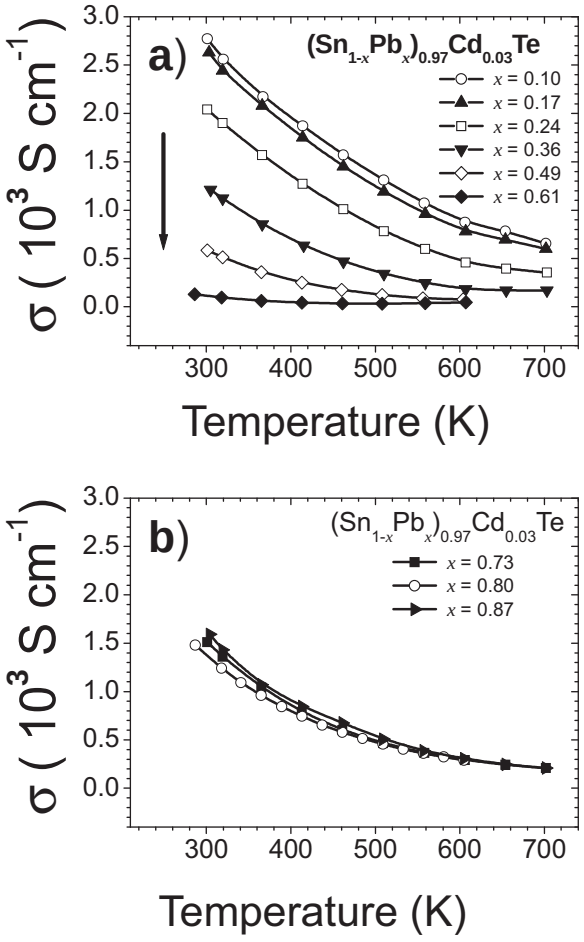

Figure 4. Temperature dependence of electrical conductivity of $(Sn_{1-x}Pb_x)_{0.97}Cd_{0.03}Te$ a) p-type; b) n-type.

The electrical conductivity decreases with increasing temperature, which is consistent with the behavior of a heavily doped degenerate semiconductor. In the Cd containing $Sn_{1-x}Pb_xTe$ system, the Seebeck coefficient depends on the Pb/Sn ratio, and can be summarized as follows: (1) For samples of $(Sn_{1-x}\ Pb_x)_{0.97}Cd_{0.03}Te$ ($0.10 \le x \le 0.49$), the Seebeck coefficient shows positive values in the whole temperature range, indicating that the holes are the dominant carriers at all temperatures. The magnitude of the Seebeck coefficient initially increases and reaches a maximum that is strongly dependent on the Pb content x. The onset of intrinsic conduction (the maxima of the curves) in these samples shifts to lower temperature with increasing Pb content, suggesting a strong compensation by minority electrons and consequently reduced concentration of holes. (2) The sample with $x = 0.61$ has a maximum at low enough temperature (~400 K) so that upon a further increase of temperature the sample undergoes a crossover to n-type conduction beginning at 500 K. These results clearly indicate a delicate balance between the positive and negative types of carriers that is expected in a material with a very small band gap ($E_g \sim 0.05$ eV), see Figure 2. (3) Samples of $(Sn_{1-x}Pb_x)_{0.97}Cd_{0.03}Te$ with $x \ge 0.73$ have negative Seebeck coefficients in the entire temperature range, indicating that the dominant charge carriers are electrons. The absolute value of Seebeck coefficient in these n-type samples increases with temperature and reaches values in excess of $-250\ \mu V\ K^{-1}$ above 700 K. The difference of the temperature dependence of electrical conductivity and Seebeck coefficient between the present Cd containing and $Pb_{1-x}Sn_xTe$ system[9] is mainly related to changes in the carrier concentration by adding the PbI_2 dopant.

The electrical conductivity and Seebeck coefficient values were used to calculate the power factor, $S^2\sigma$, shown in **Figure 6**. The power factor initially increases, reaches a maximum and then diminishes. In the p-type range of solid solutions ($0.10 \le x \le 0.61$), the maximum value of the power factor (~17 $\mu W\ cm^{-1}\ K^{-2}$) is observed at $x = 0.17$ and the power factor decreases with the increasing content of PbTe. The position of the maximum on the power factor directly reflects the position of the maximum on the Seebeck coefficient. In the n-type range of conduction, $x \ge 0.73$, the power factor is a weak function of Pb fraction and much less sensitive to the temperature. The highest power factor values reach about 21 $\mu W\ cm^{-1}\ K^{-2}$ at ~700 K for $x = 0.87$. As shown in Figure 6, the Cd containing samples show higher power factors than similar x values of undoped $Sn_{1-x}Pb_xTe$ samples. It is clear from these results that the addition of Cd causes a significant enhancement in the power factor as predicted by electronic structure calculations.[12]

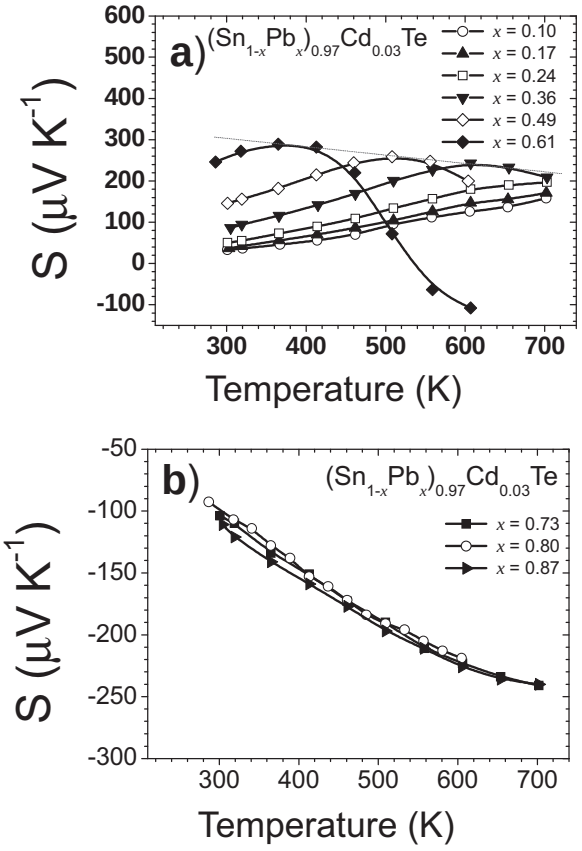

Figure 5. Temperature dependence of Seebeck coefficient of $(Sn_{1-x}Pb_x)_{0.97}Cd_{0.03}Te$ ($0.10 \le x \le 0.87$) a) p-type; b) n-type. The dashed line indicates the trend of the maximum of Seebeck coefficient.

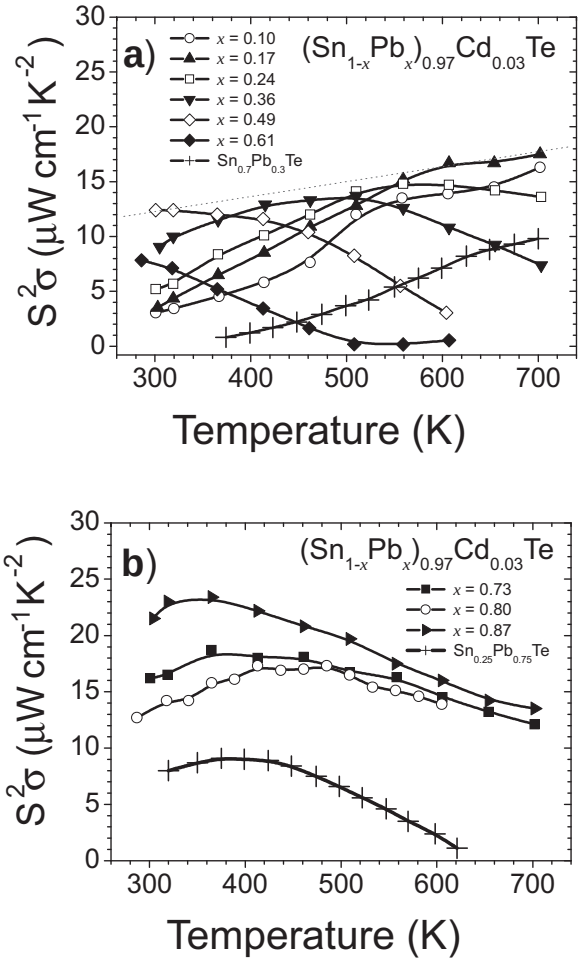

Figure 6. Temperature dependence of power factor of $(Sn_{1-x}Pb_x)_{0.97}Cd_{0.03}Te$ ($0.10 \le x \le 0.87$) a) p-type. A very well defined maximum can be observed for each sample and indicated with the dashed line. A comparison is given to power factor data published for $Sn_{0.7}Pb_{0.3}Te$ (presented as + symbol);[16] b) n-type. A comparison is given to power factor data published for $Sn_{0.25}Pb_{0.75}Te$ (presented as + symbol).[15]

Hall measurements were carried out as a function of temperature. The sign of the Hall voltage was changed depending on the composition, which is in agreement with the sign of the Seebeck coefficient data described above. Assuming one carrier type and parabolic bands in our analysis, carrier concentration (n) was calculated from the room temperature (i.e., well within a single-carrier dominated transport) Hall constants using the relationship $R_H = 1/ne$, where R_H is the Hall coefficient, n is the carrier concentration, and e is the electronic charge. Some physical properties of $(Sn_{1-x}Pb_x)_{0.97}Cd_{0.03}Te$ ($0.10 \le x \le 0.87$) in comparison with that of PbTe, SnTe[17] and undoped $Pb_xSn_{1-x}Te$[9,19] are listed in **Table 1**. The measured carrier concentration of p-type $Sn_{0.61}Pb_{0.36}Cd_{0.03}Te$ is of the order of ~10^{19} cm^{-3} which is about one order of magnitude smaller than that of corresponding $Sn_{0.6}Pb_{0.4}Te$ (p-type: ~10^{20} cm^{-3}). M. Orihashi, et al. reported that the carrier concentration decreases steadily with increasing Pb fraction for p-type $Sn_xPb_{1-x}Te$ materials grown by the Bridgman method.[9] Similarly, in our Cd containing $Sn_xPb_{1-x}Te$, the hole concentration also decreases with the increasing content of Pb. However, at $x > 0.6$, n-type behavior sets in and the concentration of electrons increases further with Pb content for a given amount of PbI_2.

Figure 7 shows the variation of mobility μ with temperature on a logarithmic scale. Hall mobilities of all $(Sn_{1-x}Pb_x)_{0.97}Cd_{0.03}Te$ samples decrease sharply above ~100 K. The power law dependence of $\mu \sim T^{-\gamma}$ was observed and the value of the exponent is listed in Table 1. The value of the exponent is related to the contribution of acoustic phonon scattering at the Pb-rich side of composition near 300 K. In contrast, the Sn-rich side of the compositions shows slower temperature variation (i.e. lower exponent), suggesting that, in addition to acoustic phonon scattering, there are additional scattering mechanisms, such as impurity scattering that are at play. PbTe-rich samples ($x = 0.73$, 0.80, and 0.87) have relatively higher mobility than SnTe-rich samples ($x = 0.10$, 0.36, and 0.49), as shown in Table 1.

In **Figure 8**, the absolute values of Seebeck coefficient of samples at 300 K versus carrier concentration are plotted on the so-called Pisarenko plot for bulk PbTe in order to see whether the Seebeck coefficient of samples is enhanced at the same carrier concentration. Our samples nearly follow the Pisarenko plot, and no significant enhancement of the Seebeck coefficient is observed within the given amount of PbI_2 doping. This indicates that the Cd resonance level either does not form or is not accessed at these carrier concentrations, the result which is consistent with previous studies of the $Pb_{1-x}Cd_xTe$ system.

Table 1. Charge transport properties of $(Sn_{1-x}Pb_x)_{0.97}Cd_{0.03}Te$ at 300K.[a)]

Pb, x	Type	n [cm^{-3}]	Mobility [$cm^2V^{-1}s^{-1}$]	S [$\mu V\ K^{-1}$]	γ	Ref.
SnTe	p	6.0×10^{20}	500	39		
PbTe	n	5.0×10^{18}	1500	280		
Un-doped Pb_xSn_xTe						
0.4	p	2.7×10^{20}		5		9
0.8	p	3.1×10^{20}		120		9
Cd-doped Pb_xSn_xTe						
0.10	p	1.7×10^{20}	82	32.94	–0.3	This work
0.36	p	3.1×10^{19}	165	85.86	–0.9	This work
0.49	p	0.8×10^{19}	310	145.23	–1.8	This work
0.73	n	1.4×10^{19}	620	–103.21	–1.5	This work
0.80	n	1.6×10^{19}	524	–91.78	–1.6	This work
0.87	n	2.2×10^{19}	595	–110.02	–1.2	This work

[a)]0.055 mol% PbI_2 was used as n-type dopant in $(Sn_{1-x}Pb_x)_{0.97}Cd_{0.03}Te$ system.

2.2. Lattice Thermal Conductivity and Thermoelectric Figure of Merit

Figure 9 shows the temperature dependence of the thermal conductivity of $(Sn_{1-x}Pb_x)_{0.97}Cd_{0.03}Te$ samples. In all cases, the total thermal conductivity κ_{tot} decreased with increasing temperature. As a function of x, the total thermal conductivity decreases up to value of x = 0.61 and then increases as the concentration of Pb increases. The total thermal conductivity (κ_{tot}) is the sum of two contributions, one from the charge carriers (κ_{elec}), and the other from the lattice vibrations (κ_{latt}), $\kappa_{tot} = \kappa_{elec} + \kappa_{latt}$. Here κ_{elec} is expressed via the Wiedemann-Franz law, $\kappa_{elec} = L\cdot\sigma\cdot T$, where L is the Lorenz number and T the absolute temperature. The value of the Lorenz number for $Pb_{0.95}Sn_{0.5}Te$ ($L = 1.73\times10^{-8}\ V^2\ K^{-2}$)[20] was used to estimate κ_{elec}. The κ_{latt} values were calculated by subtracting κ_{elec} from κ_{tot} and presented in **Figure 10**. The κ_{latt} values of the $(Sn_{1-x}Pb_x)_{0.97}Cd_{0.03}Te$ samples generally have low values in the range 0.5 ~ 2.2 W m^{-1} K^{-1} at 300 K, which is depressed well below that of pure PbTe (κ_{latt} ~ 2.3 W m^{-1} K^{-1} at 300 K). Shown in Figure 10, κ_{latt} value initially decreases, reaches a minimum and then increases due to the contribution of a bipolar term into the thermal conductivity. In the n-type range of solid solutions, κ_{latt} values at 300 K of 0.5, 0.7,

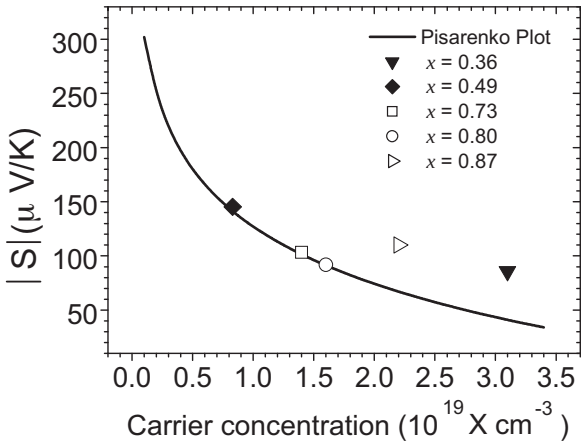

Figure 8. Absolute value of the Seebeck coefficient of various samples as a function of carrier concentration at room temperature.

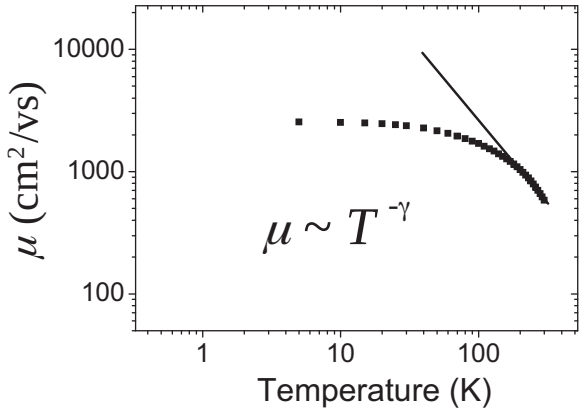

Figure 7. Temperature dependence of mobility μ for $(Sn_{1-x}Pb_x)_{0.97}Cd_{0.03}Te$ samples. The power law dependence of $\mu \sim T^{-\gamma}$ was observed and the value of the exponent is listed in Table 1.

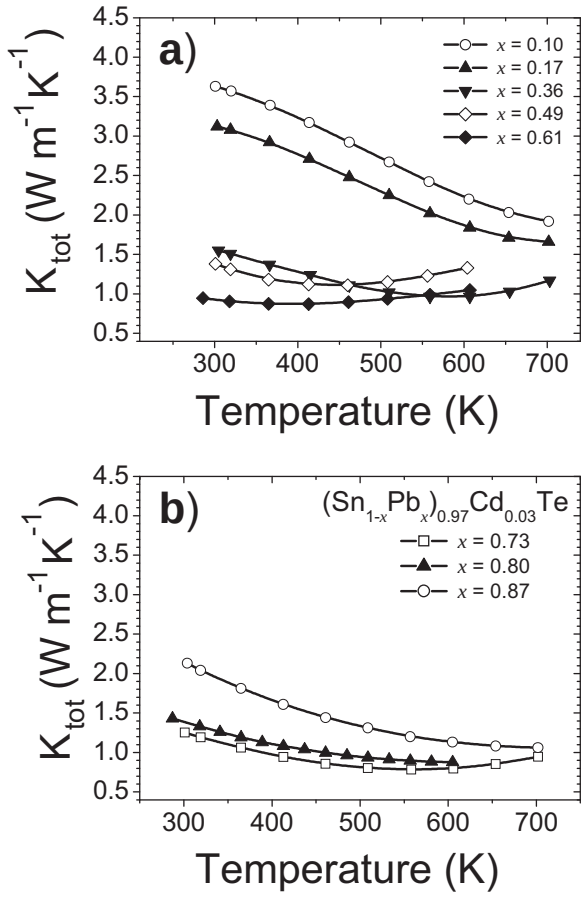

Figure 9. Variation of total thermal conductivities of $(Sn_{1-x}Pb_x)_{0.97}Cd_{0.03}Te$ ($0.10 \le x \le 0.87$) a) p-type; b) n-type. Notation and symbols are the same as those in Figure 5.

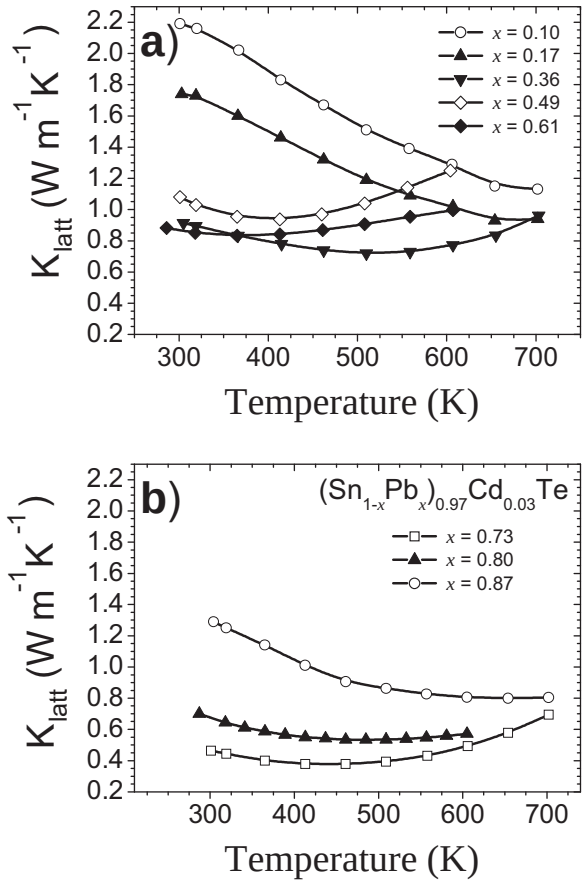

Figure 10. Variation of lattice thermal conductivities of $(Sn_{1-x}Pb_x)_{0.97}Cd_{0.03}Te$ ($0.10 \le x \le 0.87$) a) p-type; b) n-type. Notation and symbols are the same as those in Figure 5.

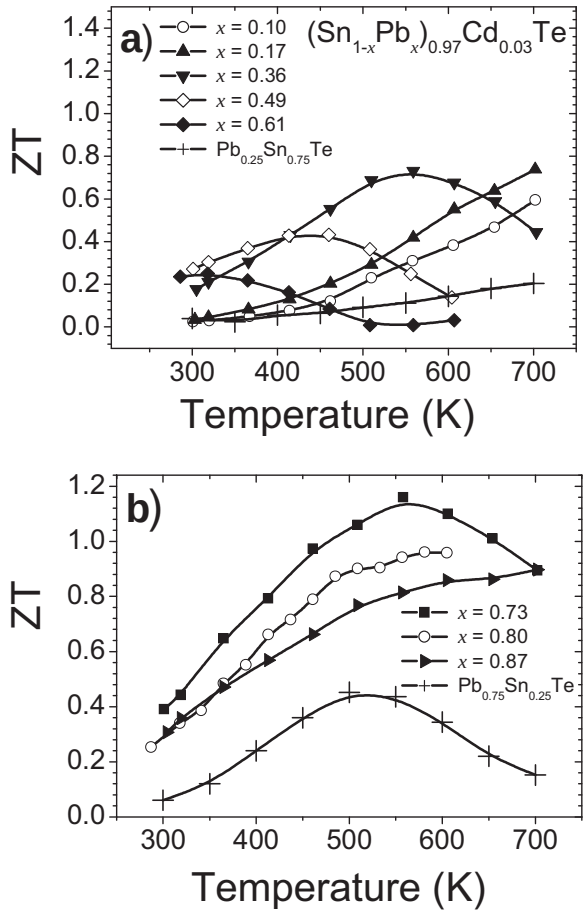

Figure 11. Temperature dependence of the thermoelectric figure of merit of $(Sn_{1-x}Pb_x)_{0.97}Cd_{0.03}Te$ ($0.10 \le x \le 0.87$) a) p-type; A comparison is given to ZT data published for undoped $Pb_{0.25}Sn_{0.75}Te$ (presented as + symbol) from reference;[9] b) n-type. A comparison is given to ZT data published for $Pb_{0.75}Sn_{0.25}Te$ (presented as + symbol).[9]

and 1.29 W m^{-1} K^{-1} were observed for x = 0.73, 0.80 and 0.87, respectively. These values are lower than the room temperature values of $Sn_{1-x}Pb_xTe$ which show 1.12, 1.03 and 1.33 W m^{-1} K^{-1} for x values of 0.5, 0.75 and 0.9, respectively.[15] Regardless of the exact mechanism, Cd appears to play a role in lowering the lattice thermal conductivity. The $Pb_{1-x}Cd_xTe$ system shows well-developed nanostructuring with extensive and diverse inhomogeneities arising from the nucleation and growth of CdTe nanocrystals. This suggests that comparable nanoscale inhomogeneities, likely are present in the $(Sn_{1-x}Pb_x)_{0.97}Cd_{0.03}Te$ systems as well.[13]

Figure 11 shows temperature dependences of ZT for the $(Sn_{1-x}Pb_x)_{0.97}Cd_{0.03}Te$ samples. For p-type materials, *ZT* initially increases, reaches a maximum and then falls with the increasing Pb content (shown in Figure 11(a)). The ZT maximum shifts to lower temperatures with increasing Pb concentration and diminishes in magnitude as a consequence of the early onset of intrinsic conduction. For the p-type samples, the maximum ZT ~ 0.7 was observed for x = 0.36 at 560 K. Much higher values (ZT ~ 1.2 at 560 K for x = 0.73, shown in Figure 11(b)) were obtained on n-type samples, which benefit primarily from a lower carrier concentration and a strongly suppressed lattice thermal conductivity. The ZT values observed in the present study are much higher that those reported in the literature for samples of the same Sn/Pb ratio (ZT ~ 0.56 for p-type $Pb_{0.4}Sn_{0.6}Te$ at 700 K, and ZT ~ 0.46 for n-type $Pb_{0.75}Sn_{0.25}Te$ at 510 K).[9]

3. Conclusions

The effect of Pb/Sn ratio on the thermoelectric properties of Cd containing $Sn_{1-x}Pb_xTe$ is significant. We have shown that Cd plays an active role in reducing the carrier concentration, altering physical properties and changing the charge transport type in $Sn_{1-x}Pb_xTe$. The power factor of the Cd-containing samples is about twice as large as that in the case of the corresponding $Sn_{1-x}Pb_xTe$ samples.

The κ_{latt} values of the $(Sn_{1-x}Pb_x)_{0.97}Cd_{0.03}Te$ samples are low and in the range 0.5 ~ 2.2 W m^{-1} K^{-1} at 300 K. These are well below that of pure PbTe (κ_{latt} value ~ 2.3 W m^{-1} K^{-1} at 300 K) and that of undoped $Sn_{1-x}Pb_xTe$ (κ_{latt} value ~ 1.12, 1.03 and 1.33 W m^{-1} K^{-1} for x values of 0.5, 0.75 and 0.9, respectively). Therefore, the higher power factor, together with the lower thermal conductivity results in higher ZT for

$(Sn_{1-x}Pb_x)_{0.97}Cd_{0.03}Te$ than that of undoped $Sn_{1-x}Pb_xTe$. The maximum ZT (~ 0.7) values are observed for the p-type material with x = 0.36 at 560 K. Much higher values (ZT ~ 1.2 at 560 K for x = 0.73) are obtained on n-type samples.

4. Experimental Section

Synthesis: $(Sn_{1-x}Pb_x)_{0.97}Cd_{0.03}Te$ ($0.10 \leq x \leq 0.87$) samples with PbI_2 dopant, each with a total mass of ca. 7 ~ 10 g, were prepared by mixing appropriate stoichiometric ratios of high purity starting elemental materials, namely Pb, Sn, Cd and Te (>99.9% in purity). The 0.055 mol% PbI_2 dopant compositions were chosen according to the reported data[7] regarding optimization of ZT for the standard $Sn_{1-x}Pb_xTe$ materials. Note that, in this study, the mole fraction of CdTe was fixed to 3% which is believed to be close to its maximum solubility in the lattice. Stoichiometric amounts of Pb, Sn, Cd and Te were loaded into evacuated carbon-coated silica tubes (10 mm diameter, 1mm wall thickness) and then sealed under a residual pressure of ~10^{-4} Torr to prevent oxidation at high temperatures. The sealed tubes were heated to 1050 °C over 16 h and then held there for 5 h while rocking the liquid to facilitate complete mixing of the constituents. The final step consisted of two parts: (1) cool down to 750 °C over 2 h and then held there for 4 h, (2) cool down from 750 °C to room temperature over 18 h. The resulting dense ingots had a dark silvery metallic shine. The ingots are stable in water and air.

Powder X-ray Diffraction: The powder diffraction patterns were obtained with an Inel diffractometer equipped with a position sensitive detector and operating at 40 kV and 20 mA. Data acquisition was controlled via the *In-Situ* program. The lattice parameters of $(Sn_{1-x}Pb_x)_{0.97}Cd_{0.03}Te$ ($0.10 \leq x \leq 0.87$) samples were obtained from least squares refinement of data in the range of 2θ between 20° and 80° with the aid of a *Rietveld* refinement program.[21] X-ray powder diffraction patterns showed a single phase products crystallizing in a cubic F lattice (NaCl-type).

Thermal Conductivity: The thermal diffusivity (D) was determined by the flash diffusivity-heat capacity method using NETZSCH LFA 457 MicroFlash instrument under a nitrogen atmosphere, and specific heat (C_p) was indirectly derived using a standard sample (Pyroceram) as a function of temperature from room temperature to ~700 K. In the flash method, the front face of a disc-shaped plane-parallel (8 mm or 13 mm diameter; 1 ~ 2 mm thickness) surface was heated by a short energy pulse, e.g. a laser beam. Thermal response on the rear surface was monitored by IR detector. The thermal conductivity (κ_{tot}) was calculated from the equation $\kappa_{tot} = D \cdot C_p \cdot \rho$, where the sample density ρ was measured using the sample's geometry and mass.

Electrical Properties: For measurements of electrical properties, samples were cut in the shape of rectangle of about $3 \times 3 \times 8$ mm^3. Electrical conductivity and Seebeck coefficient were measured simultaneously at helium atmosphere from room temperature to about 650 K using a ULVAC-RIKO ZEM-3. The electrical conductivity was measured using 4 probe methods. The Seebeck coefficients were measured 3 times with different temperature gradient in the range 5 – 15 K at each temperature step.

Infrared Spectroscopy: To probe the optical energy band gap of the series, room temperature optical diffuse reflectance measurements were performed using a Nicolet 6700 FTIR spectrometer. The spectra were monitored in the mid-IR region (6000–400 cm^{-1}). Absorption data were calculated from reflectance data using the Kubelka-Munk function. The optical band gaps were derived from absorption versus E (eV) plots.[22]

Hall Measurements: The Hall effects were measured using a Quantum Design MPMS (magnetic property measurement system) with the aid of a Linear Research AC bridge operating at 16 Hz excitation. Within the MPMS Dewar, a cryogenic probe integrates a five Tesla superconducting magnet with a SQUID detection system. The data was collected over the temperature range from 1.9 K to 300 K. Four-wire AC Hall measurements were performed on parallelepiped samples with the typical size of $1 \times 3 \times 5$ mm^3. Fine copper wires were used as the current and Hall voltage leads and the contacts were made using an indium solder.

Acknowledgements

This work was supported as part of the Revolutionary Materials for Solid State Energy Conversion, an Energy Frontier Research Center funded by the U.S. Department of Energy, Office of Science, Office of Basic Energy Sciences under Award Number DE-SC0001054. M.-K. Han. and S.-J. Kim acknowledge financial support from the Basic Science Research Program through the National Research Foundation of Korea (20110003767) and Nano Material Technology Development Program through the National Research Foundation of Korea(NRF) funded by the Ministry of Education, Science and Technology (20110030147), Korea.

Received: February 4, 2012
Published online: June 16, 2012

[1] a) J. R. Sootsman, D. Y. Chung, M. G. Kanatzidis, *Angew. Chem. Int. Ed.* **2009**, *48*, 8616; b) M. G. Kanatzidis, *Chem. Mater.* **2010**, *22*, 648.
[2] a) G. J. Snyder, E. S. Toberer, *Nat. Mater.* **2008**, *7*, 105; b) L. E. Bell, *Science* **2008**, *321*, 1457; c) C. J. Vineis, A. Shakouri, A. Majumdar, M. G. Kanatzidis, *Adv. Mater.* **2010**, *22*, 3970.
[3] a) K. F. Hsu, S. Loo, F. Guo, W. Chen, J. S. Dyck, C. Uher, T. Hogan, E. K. Polychroniadis, M. G. Kanatzidis, *Science* **2004**, *303*, 818; b) J. Androulakis, I. Todorov, D. Y. Chung, S. Ballikaya, G. Y. Wang, C. Uher, M. G. Kanatzidis, *Phys. Rev. B* **2010**, *82*, 115209; c) M.-K. Han, J. Androulakis, S.-J. Kim, M. G. Kanatzidis, *Adv. Energy Mater.* **2012**, *2*, 157; d) L.-D. Zhao, S.-H. Lo, J. He, H. Li, K. Biswas, J. Androulakis, C. Wu, T. P. Hogan, D.-Y. Chung, V. P. Dravid, M. G. Kanatzidis, *J. Am. Chem. Soc.* **2011**, *133*, 20476.
[4] a) D. M. Rowe, C. M. Bhandari, *Appl. Phys. Lett.* **1985**, *47*, 255; b) J. P. Heremans, V. Jovovic, E. S. Toberer, A. Saramat, K. Kurosaki, A. Charoenphakdee, S. Yamanaka, G. J. Snyder, *Science* **2008**, *321*, 554; c) Y. Z. Pei, X. Y. Shi, A. LaLonde, H. Wang, L. D. Chen, G. J. Snyder, *Nature* **2011**, *473*, 66.
[5] C. Wood, *Reports on Progress in Physics* **1988**, *51*, 459.
[6] a) M.-K. Han, K. Hoang, H. J. Kong, R. Pcionek, C. Uher, K. M. Paraskevopoulos, S. D. Mahanti, M. G. Kanatzidis, *Chem. Mater.* **2008**, *20*, 3512; b) J. Androulakis, K.-F. Hsu, R. Pcionek, H. Kong, C. Uher, J. J. D'Angelo, A. Downey, T. Hogan, M. G. Kanatzidis, *Adv. Mater.* **2006**, *18*, 1170; c) A. Gueguen, P. F. P. Poudeu, C. P. Li, S. Moses, C. Uher, J. Q. He, V. Dravid, K. A. Paraskevopoulous, M. G. Kanatzidis, *Chem. Mater.* **2009**, *21*, 1683; d) Y. Z. Pei, A. F. May, G. J. Snyder, *Adv. Energy Mater.* **2011**, *1*, 291.
[7] a) J. W. Wagner, R. K. Willardson, *Trans. Metall. Soc. AIME* **1968**, *242*, 366; b) A. A. Machonis, I. B. Cadoff, *Trans. Metall. Soc. AIME* **1964**, *230*, 333; c) E. Abramof, S. O. Ferreira, P. H. O. Rappl, H. Closs, I. N. Bandeira, *J. Appl. Phys.* **1997**, *82*, 2405; d) V. Jovovic, S. J. Thiagarajan, J. P. Heremans, T. Komissarova, D. Khokhlov, A. Nicorici, *J. Appl. Phys.* **2008**, *103*, 053710.
[8] a) Y. Gelbstein, *J. Electronic Mater.* **2011**, *40*, 533; b) I. U. Arachchige, M. G. Kanatzidis, *Nano Lett.* **2009**, *9*, 1583; c) M. K. Han, J. Androulakis, S. J. Kim, M. G. Kanatzidis, *Adv. Energy Materi.* **2012**, *2*, 157.
[9] a) M. Orihashi, Y. Noda, L.-D. Chen, T. Goto, T. Hirai, *J. Phys. Chem. Solids* **2000**, *61*, 919; b) J. L. Cui, X. Qian, X. B. Zhao, *J. Alloys Compds.* **2003**, *358*, 228.
[10] M. Ocio, *Phys. Rev. B* **1974**, *10*, 4274.
[11] J. W. Wagner, A. G. Thompson, R. K. Willardson, *J. Appl. Phys.* **1971**, *42*, 2515.
[12] S. Ahmad, S. D. Mahanti, K. Hoang, M. G. Kanatzidis, *Phys. Rev. B* **2006**, *74*, 155205.
[13] K. Ahn, M.-K. Han, J. Q. He, J. Androulakis, S. Ballikaya, C. Uber, V. P. Dravid, M. G. Kanatzdis, *J. Am. Chem. Soc.* **2010**, *132*, 5227.

[14] J. E. Huheey, E. A. Keiter, R. L. Keither, *Inorganic Chemistry: Principles of Structure and Reactivity*, 4th ed., HarperCollins, New York, USA **1993**.
[15] Y. Gelbstein, Z. Dashevsky, M. P. Dariel, *Physica B* **2007**, *391*, 256.
[16] J. O. Dimmock, I. Melngailis, A. J. Strauss, *Phys. Rev. Lett.* **1966**, *16*, 1193.
[17] R. F. Bis, J. R. Dixon, *J. Appl. Phys.* **1969**, *40*, 1918.
[18] E. G. Bylander, *Mater. Sci. Eng.* **1966**, *1*, 190.
[19] E. Silberg, A. Zemel, *J. Phys. D: Appl. Phys.* **1982**, *15*, 275.
[20] G. S. Kumar, G. Prasad, R. O. Pohl, *J. Mater. Sci.* **1993**, *28*, 4261.
[21] B. A. Hunter, C. J. Howard, *Rietica; Australian Nuclear Science and Technology Organization*, Menai, Australia **2000**.
[22] a) W. W. Wendlandt, H. G. Hecht, *Reflectance Spectroscopy*, Interscience Publishers, New York, USA **1966**; b) G. Kotuem, *Reflectance Spectroscopy*, Springer-Verlag, New York, USA **1969**; c) S. P. Tandon, J. P. Gupta, *Physica Status Solidi* **1970**, *38*, 363; d) M. G. Kanatzdis, T. H. McCarthy, T. A. Tanzer, L. H. Chen, L. Iordanidis, T. Hogan, C. R. Kannewurf, C. Uher, B. X. Chen, *Chem. Mater.* **1996**, *8*, 1465; e) J. H. Liao, M. G. Kanatzdis, *Chem. Mater.* **1993**, 5, 1561.